Interfacial Electron Transfer to the Zeolite-Encapsulated Methylviologen Acceptor from Various Carbonylmanganate Donors. Shape Selectivity of Cations in Mediating Electron Conduction through the Zeolite Framework

K. B. Yoon,* Y. S. Park, and J. K. Kochi*

Contribution from the Departments of Chemistry, Sogang University, Seoul 121-742, Korea, and University of Houston, Houston, Texas 77204-5641

Received July 30, 1996. Revised Manuscript Received October 7, 1996[⊗]

Abstract: The series of (one-electron) reductions of methylviologen (MV^{2+}) intercalated into zeolite-**Y** by various carbonylmanganate donors [$C^+Mn(CO)_4L^-$, L = CO, $P(OPh)_3$] are very selective and highly dependent on the size/shape of the counterion C^+, although the same electron transfers carried out (homogeneously) in solution always occur spontaneously, irregardless of C^+. For example, the complete reduction of MV^{2+} extensively doped into zeolite-**Y** proceeds rapidly and quantitatively when the Na^+ salts of the carbonylmanganates are employed as the reductants, but only to a very limited extent (1%) when the large PPN^+ [bis(triphenylphosphine)iminium] salts of the carbonylmanganates are employed. The medium-size tetraethylammonium (TEA^+) salt of $Mn(CO)_4P(OPh)_3^-$ slowly effects an intermediate conversion (80%). Based on the fact that the large phosphite-substituted $Mn(CO)_4P(OPh)_3^-$ donor cannot enter the supercage of zeolite-**Y**, we propose interfacial electron transfer from the carbonylmanganate to the MV^{2+} acceptor to occur only at the zeolite periphery. Importantly, the strong dependence of the further progress of the redox reaction with decreasing size of the cation C^+ (*i.e.*, shape selectivity) predicts that electron conduction throughout the zeolite framework requires the simultaneous transport of these cations in order to effect the complete reduction of all the encapsulated MV^{2+}, as presented in Chart 5.

Introduction

Zeolites are microcrystalline hosts to a wide variety of different guests, including both neutral molecules as well as charged ions.[1,2] Indeed, the ready cation exchanges of the widely available sodium zeolites have led to a series of interesting nanostructures extensively doped with (complexed) inorganic and organic cations.[3−12] Such an intercalation of redox-active cations offers us the opportunity to examine the interesting question as to how interfacial electron transfer between an electron donor (dissolved in solution) and an electron acceptor (immobilized in an insoluble matrix) is brought about. In a more general context, this mechanistic problem is also encountered in the oxidation−reduction of such diverse systems as an active center deeply embedded in a metalloenzyme or a metal-doped microheterogeneous catalyst, in which one of the partners of the redox couple does not enjoy the usual diffusive mobility inherent to homogeneous electron transfers. As such, we now inquire as to what structural factors control the interfacial electron transfer in order to identify the sequence of steps by which the electron is transported from the bulk solution into the interior of the solid phase. To address these questions, we rely on (a) crystalline zeolites to provide a well-defined steric environment for the encapsulated (cationic) acceptor and (b) anionic donors A^- of varying shapes which coupled with differently sized counterions C^+ provide a series of graded salts [C^+A^-] to modulate the interfacial electron transfer.

Our initial model system as described in this study is based on zeolite-Y as the molecular compartment, and methylviologen (MV^{2+} = *N*,*N*′-dimethyl-4,4′-bipyridinium) is selected as the prototypical electron acceptor for the following reasons. First, the physicochemical properties of MV^{2+}, including its redox behavior in various solutions, have been extensively studied.[13−17] For example, the colorless methylviologen ($\lambda_{max} \sim 260$ nm)[13] turns intense blue (molar extinction coefficient at 605 nm is

[⊗] Abstract published in *Advance ACS Abstracts,* December 1, 1996.

(1) (a) Breck, D. W. *Zeolite Molecular Sieves*; Wiley: New York, 1974. (b) Barrer, R. M. *Zeolites and Clay Minerals as Sorbents and Molecular Sieves*: Academic: London, 1978.

(2) Yoon, K. B. *Chem. Rev.* **1993**, *93*, 321.

(3) (a) Yonemoto, E. H.; Kim, Y. I.; Schmehl, R. H.; Wallin, J. O.; Shoulders, B. A.; Richardson, B. R.; Haw, J. F.; Mallouk, T. E. *J. Am. Chem. Soc*. **1994**, *116*, 10557. (b) Kim, Y. I.; Mallouk, T. E. *J. Phys. Chem*. **1992**, *96*, 2879. (c) Krueger, J. S.; Mayer, J. E.; Mallouk, T. E. *J. Am. Chem. Soc*. **1988**, *110*, 8232. (d) Persaud, L.; Bard, A. J.; Campion, A.; Fox, M. A.; Mallouk, T. E.; Webber, S. E.; White, J. M. *J. Am. Chem. Soc*. **1987**, *109*, 7309.

(4) (a) Borja, M.; Dutta, P. K. *Nature* **1993**, *362*, 43. (b) Dutta, P. K.; Incavo, J. A. *J. Phys. Chem*. **1987**, *91*, 4443. (c) Dutta, P. K.; Turbeville, W. *J. Phys. Chem*. **1992**, *96*, 9410. (d) Dutta, P. K.; Borja, M. *J. Chem. Soc., Chem. Commun*. **1993**, 1568. (e) Ledney, M.; Dutta, P. K. *J. Am. Chem. Soc*. **1995**, *117*, 7687.

(5) Fukuzumi, S.; Urano, T.; Suenobu, T. *Chem. Commun*. **1996**, 213.

(6) Corma, A.; Fornés, V.; Garcia, H.; Miranda, M. A.; Primo, J.; Sabater, M.-J. *J. Am. Chem. Soc*. **1994**, *116*, 2276.

(7) (a) Sankararaman, S.; Yoon, K. B.; Yabe, T.; Kochi, J. K. *J. Am. Chem. Soc*. **1991**, *113*, 1419. (b) Yoon, K. B.; Hubig, S. M.; Kochi, J. K. *J. Phys. Chem*. **1994**, *98*, 3865.

(8) (a) Rolison, D. R. *Chem. Rev*. **1990**, *90*, 867. (b) Rolison, D. R. *Stud. Surf. Sci. Catal*. **1994**, *85*, 543.

(9) (a) Calzaferri, G.; Lanz, M.; Li, J. *J. Chem. Soc., Chem. Commun*. **1995**, 1313. (b) Li, J.; Pfanner, K.; Calzaferri, G. *J. Phys. Chem*. **1995**, *99*, 2119. (c) Li, J.; Calzaferri, G. *J. Electroanal. Chem*. **1994**, *377*, 163. (d) Li, J.; Calzaferri, G. *J. Chem. Soc., Chem. Commun*. **1993**, 1430.

(10) (a) Walcarius, A.; Lamberts, L.; Derouane, E. G. *Electrochim. Acta* **1993**, *38*, 2257. (b) Walcarius, A.; Lamberts, L.; Derouane, E. G. *Ibid*. **1993**, *38*, 2267.

(11) Gemborys, H. A.; Shaw, B. R. *J. Electroanal. Chem. Interfacial Electrochem*. **1986**, *208*, 95.

(12) Grätzel, M.; Kalyanasundaram, K. Eds.; *Kinetics and Catalysis in Microheterogeneous Systems*; Marcel Dekker: New York, 1991.

(13) Summers, R. A. *The Bipyridinium Herbicides*; Academic: New York, 1980.

(14) (a) Kosower, E. M.; Cotter, L. J. *J. Am. Chem. Soc*. **1964**, *86*, 5524. (b) Farrington, J. A.; Ebert, M.; Land, E. J. *J. Chem. Soc., Faraday Trans. 1*, **1978**, *74*, 665. (c) Farrington, J. A.; Ebert, M.; Land, E. J.; Fletcher, K. *Biochim. Biophys. Acta* **1973**, *314*, 372.

S0002-7863(96)02645-5 CCC: $12.00

Chart 1. Perspective showing the snug fit of methylviologen within the 13 Å supercage of zeolite-Y.

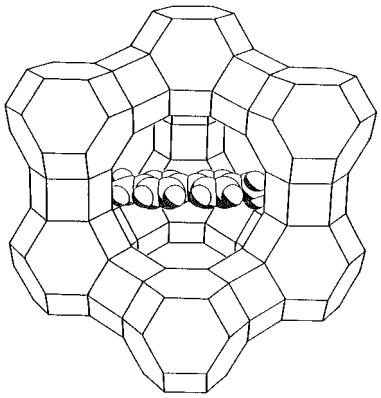

Chart 2. Ready passage of $Mn(CO)_5^-$ through the 7.4 Å aperture of zeolite-**Y** which precludes the admission of the phosphite-substituted $Mn(CO)_4P(OPh)_3^-$ shown to the right on the same scale.

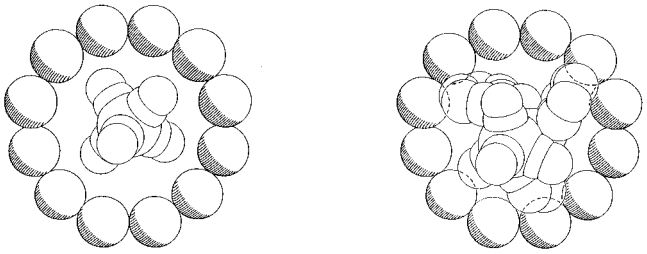

$\sim$14 000)[16] upon one-electron reduction, so that methylviologen cation radical ($MV^{\bullet+}$) is readily distinguished from its dicationic state (MV^{2+}). Thus, the progress of the redox reaction can be easily monitored both visually (qualitatively) and spectrophotometrically (quantitatively). Second, methylviologen can be readily incorporated into various zeolites via simple aqueous ion exchanges,[2−4,8−11] and Chart 1 presents the perspective view of MV^{2+} intercalated within the quasi-spherical (13 Å) supercage of zeolite-**Y**. Third, the incorporation of methylviologen can be accurately controlled so that the occupancy in each supercage is limited to an average of either one or two MV^{2+}, hereafter designated as MV(1.0)**Y** and MV(2.0)**Y**, respectively.[18,19] Furthermore, methylviologen remains intact within the dehydrated zeolites to allow the accommodation of various other guest molecules into the remaining (void) space for subsequent intermolecular interactions.[2,18,19]

The anionic carbonylmanganates with $A^- = Mn(CO)_4L^-$ [L = CO or $P(OPh)_3$] are chosen as the prototypical electron donors based on the following factors. First, we will show that they both behave as clean (one-electron) reducing agents toward MV^{2+} both in a homogeneous solution of acetonitrile and as a heterogeneous suspension in tetrahydrofuran. Second, while $Mn(CO)_5^-$ can freely pass through the 7.4 Å aperture of zeolite-**Y**, the triphenyl phosphite-substituted analogue $Mn(CO)_4P(OPh)_3^-$ is too big to enter the pore opening,[20] and hence cannot react directly with all the encapsulated MV^{2+}. (See Chart 2 for the computer-generated perspective views of these manganates in the vicinity of the zeolite-**Y** aperture.) Thus, by simple ligand substitution, we can readily create two contrasting situations in which one donor [$Mn(CO)_4P(OPh)_3^-$] is size excluded from the zeolite, while the other donor [$Mn(CO)_5^-$] has free access into the supercage. Furthermore, one of the best advantages to be gained in using metal carbonyl anions as reducing agents is that the overall dimension of the salt is effectively controlled by the size of the charge-compensating cations (C^+), since the anionic carbonylmanganates must enter the zeolitic pores in the paired state with their counterions.[18] Therefore, by varying the size of the cations C^+ listed in Chart 3, we can further finely tune the effective size of the manganate donors.

Chart 3. Increasing steric size of the counter cations $C^+ = TMA^+ < TEA^+ < TBA^+ < PPh_4^+ < PPN^+$ used in this study.

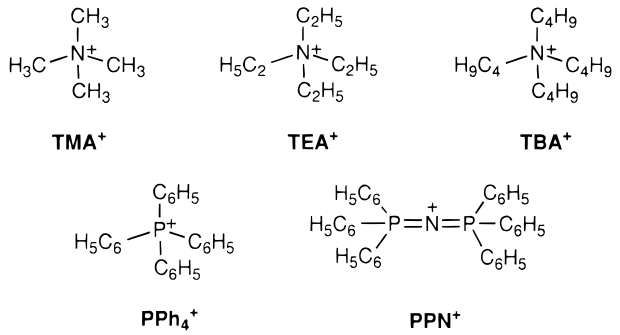

In this report, the factors that govern the interfacial electron transfer between the methylviologen acceptor encapsulated in zeolite-**Y** and the carbonylmanganate donors located externally (in solution) will be examined with different substituents (L) and various counter cations (C^+).

Results

For this investigation, we initially established that the simple methylviologen salt was always subject to rapid and quantitative (one-electron) reduction in solution, irrespective of the carbonylmanganate donor $C^+Mn(CO)_4L^-$, with L = CO and $P(OPh)_3$. Interfacial electron transfer to MV^{2+} extensively intercalated into zeolite-**Y** particles was then examined with the same series of carbonylmanganate salts comprised of different sizes/shapes of the counter cation C^+ as follows.

I. Homogeneous Electron Transfer between Various Carbonylmanganates and Methylviologen in Solution. When the bis(triphenylphosphine)iminium (PPN^+) salt of pentacarbonylmanganate $Mn(CO)_5^-$ (1 equiv) was added to an acetonitrile solution of the trifluoromethanesulfonate (OTf^-) salt of methylviologen $MV(OTf)_2$ (in the glovebox), the colorless solution immediately turned deep blue. The FT-IR analysis of the dark (inky) blue solution showed that dimanganese decacarbonyl $Mn_2(CO)_{10}$ was formed in quantitative amounts (Table 1, entry 1). The UV−vis spectrophotometric analysis of the solution also revealed the formation of methylviologen cation radical ($MV^{\bullet+}$) in the essentially quantitative amounts according to the stoichiometry in eq 1.

$$MV^{2+} + Mn(CO)_5^- \rightarrow MV^{\bullet+} + {}^1/_2Mn_2(CO)_{10} \qquad (1)$$

Similarly, the same deep blue solution was instantaneously obtained when methylviologen was treated with 1 equiv of the phosphite-substituted salt $PPN^+Mn(CO)_4P(OPh)_3^-$. The spectroscopic analyses of the blue solution revealed that the corresponding manganese dimer $Mn_2(CO)_8[P(OPh)_3]_2$ and $MV^{\bullet+}$ were also formed in quantitative amounts (see Table 1). The use of tetraethylammonium (TEA^+) and sodium (Na^+) salts of

(15) Bird, C. L.; Kuhn, A. T. *Chem. Soc. Rev.* **1981**, *10*, 49.
(16) Watanabe, T.; Honda, K. *J. Phys. Chem.* **1982**, *86*, 2617.
(17) Wolszczak, M.; Stradowski, C. *Radiat. Phys. Chem.* **1989**, *33*, 355.
(18) Yoon, K. B.; Kochi, J. K. *J. Phys. Chem.* **1991**, *95*, 1348.
(19) Yoon, K. B.; Kochi, J. K. *J. Phys. Chem.* **1991**, *95*, 3780.
(20) The kinetic diameter of $Mn(CO)_5^-$ was estimated to be 7.1 Å based on the crystal structure reported by: Corraine, M. S.; Lai, C. K.; Zhen, Y.; Churchill, M. R.; Buttrey, L. A.; Ziller, J. W.; Atwood, J. D. *Organometallics*, **1992**, *11*, 35. The kinetic diameter of $Mn(CO)_4P(OPh)_3^-$ was estimated to be $\gtrsim$10 Å based on the computer minimization.

Table 1. Homogeneous Electron Transfer between $MV^{2+}(CF_3SO_3^-)_2$ and $C^+Mn(CO)_4L^-$ [a]

solvent	C^+	L	time (h)	$Mn_2(CO)_8L_2$,[b] (conv)[c]	$MV^{\bullet+}$ [d]	(conv)[c]
CH_3CN	PPN^+	CO	0.2	0.083 (95)	0.079	(91)
CH_3CN	PPN^+	$P(OPh)_3$	0.2	0.085 (98)	0.085	(98)
CH_3CN	TEA^+	$P(OPh)_3$	0.2	0.088 (100)	0.080	(92)
CH_3CN	Na^+	$P(OPh)_3$	0.2	0.084 (97)	0.081	(93)
THF[e]	PPN^+	CO	2	0.019 (22)	—[f]	—[f]
THF[e]	PPN^+	CO	24	0.050 (58)	—[f]	—[f]
THF[e]	PPN^+	$P(OPh)_3$	2	0.040 (46)	—[f]	—[f]
THF[e]	PPN^+	$P(OPh)_3$	36	0.070 (80)	—[f]	—[f]

[a] Equimolar (0.087 mmol) amounts of $MV^{2+}(CF_3SO_3^-)_2$ and $C^+Mn(CO)_4L^-$ were mixed in 50 mL of solvent. [b] In mmol (2×). [c] In %, based on the amount (0.087 mmol) of each reactant. [d] In mmol, based on $\epsilon = 13{,}900$ at 605 nm for $MV^{\bullet+}$ in CH_3CN. [e] $MV^{2+}(CF_3SO_3^-)_2$ was insoluble in THF. [f] $MV^{\bullet+}CF_3SO_3^-$ was sparingly soluble in THF.

$Mn(CO)_4P(OPh)_3^-$ also led to the same results, and indicated that the nature of the counter cation did not affect the homogeneous redox reaction. These results clearly showed that electron transfer from the phosphite-substituted carbonylmanganates $Mn(CO)_4P(OPh)_3^-$ to MV^{2+} occurred in homogeneous (acetonitrile) solution according to the stoichiometry:

$$MV^{2+} + Mn(CO)_4P(OPh)_3^- \rightarrow MV^{\bullet+} + {}^1/_2Mn_2(CO)_8[P(OPh)_3]_2 \quad (2)$$

We thus conclude that the various carbonylmanganates can effectively serve as clean one-electron reducing agents for methylviologen.

The redox transformations were also examined in tetrahydrofuran (THF) in which $MV(OTf)_2$ was completely insoluble. Nonetheless, the same redox reactions proceeded, albeit somewhat slowly[21] as demonstrated in Table 1 by the carbonylmanganate conversions of ~60 and 80% for L = CO and $P(OPh)_3$ after 24 and 36 h, respectively.[22] The latter indicated that the redox reactions between MV^{2+} and $Mn(CO)_4L^-$ as described in eq 1 and 2 were also applicable to a THF medium, despite the quasi-heterogeneous conditions.

II. Heterogeneous Electron Transfer between the Carbonylmanganates and MV^{2+} Encapsulated in Zeolite-Y. 1. Preliminary (Qualitative) Observations. When samples of MV^{2+}-doped zeolite-**Y** suspended in either THF or acetonitrile were treated with small amounts of $C^+Mn(CO)_5^-$, the zeolite particles immediately turned varying degrees of blue, regardless of the size of the cation C^+ (see Chart 3). In striking contrast, the supernatant solution either remained colorless or turned pale yellow. Based on a qualitative (visual) inspection, the intensities of the blue zeolites were significantly weaker (especially in the dried state) when they were produced from the large TBA^+, PPh_4^+, and PPN^+ salts of $Mn(CO)_5^-$ compared to those obtained from the corresponding salts with TEA^+, TMA^+, and Na^+ as the smaller counter cations (see Chart 3). Consistent with the blue colorations, the diffuse reflectance UV−vis spectra of the filtered and dried zeolites all confirmed the presence of $MV^{\bullet+}$ within the blue zeolites (compare Figure 1). Although these tests were qualitative, the results were rather surprising to us in view of our previous studies[18] which showed that only the added salts with cations smaller than TBA^+ could successfully enter

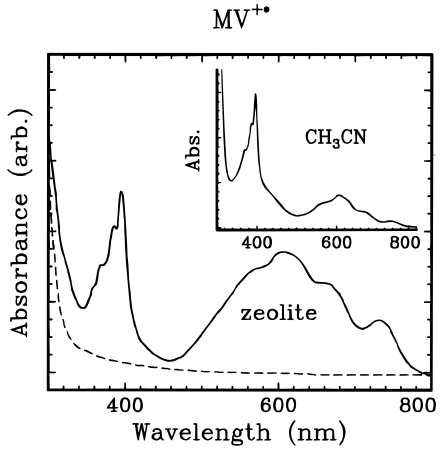

Figure 1. Comparison of the UV-vis spectrum of the methylviologen cation radical ($MV^{\bullet+}$) encapsulated in zeolite-**Y** and dissolved in acetonitrile (inset). The dashed line represents the background for the undoped zeolite-**Y**.

the supercage of zeolite-**Y** to form intermolecular charge-transfer salts with MV^{2+}. In order to accommodate these rather anomalous results, we carried out further quantitative studies as follows.

2. Quantitative Accounting of the Carbonylmanganate Oxidations by MV^{2+}-Doped Zeolite-Y. A. Oxidation of the Pentacarbonylmanganate Salts $C^+Mn(CO)_5^-$ with MV(1.0)Y. When Na^+ $Mn(CO)_5^-$ (0.069 mmol, 0.12 equiv)[23] was added to MV(1.0)**Y**[24] (0.057 mmol of MV^{2+} in 0.1 g of zeolite) suspended in THF,[25] the colorless zeolite particles immediately turned dark blue. The reaction mixture was stirred for 0.2 h, and the supernatant solution was then quantitatively collected by filtration. FT-IR analysis of the (supernatant) solution revealed the presence of only $Mn_2(CO)_{10}$ in quantitative amounts,[23] *i.e.*

$$(MV^{2+})\mathbf{Y} + Na^+Mn(CO)_5^- \xrightarrow{100\%} (Na^+MV^{\bullet+})\mathbf{Y} + {}^1/_2Mn_2(CO)_{10} \quad (3)$$

Most importantly, the diffuse reflectance UV−vis spectrum of the filtered dark blue zeolite showed the characteristic absorption band of the methylviologen cation radical ($MV^{\bullet+}$) with the high intensity shown in Figure 1. Unfortunately, the precise amount of $MV^{\bullet+}$ produced could not be accurately measured owing to the experimental difficulty of quantitatively extracting all of the highly air-sensitive $MV^{\bullet+}$ out of zeolite. However, the high intensity of $MV^{\bullet+}$ in the blue zeolite, together with the quantitative oxidation of $Mn(CO)_5^-$ to $Mn_2(CO)_{10}$, was indicative of the complete conversion of MV^{2+} to $MV^{\bullet+}$. The resulting spectrum also showed a weak broad absorption in the near infrared (NIR) region with an absorption maximum at about 1100 nm.[26]

When the $Mn(CO)_5^-$ salt with the large PPN^+ cation was added to the THF slurry of MV(1.0)**Y**, the zeolite particles also

(21) The slow redox reaction may be attributed to the low solubility of $MV^{\bullet+}OTf^-$.

(22) During the course of reactions in THF, the supernatant solution turned pale greenish blue due to the formation of yellow manganese dimers and to the partial solubility of $MV^{\bullet+}OTf^-$. The simultaneous formation of $MV^{\bullet+}OTf^-$ was inferred from the isolation of a black precipitate which afforded a dark blue solution of $MV^{\bullet+}$ upon dissolution in acetonitrile.

(23) Based on the total amount of MV^{2+} intercalated into zeolite-**Y**.

(24) The number in the parentheses represents the (average) number of MV^{2+} in the supercage.

(25) (a) For the quantitative study, we chose THF to mimic the heterogeneous redox chemistry between the MV^{2+} ions that are intercalated within zeolite-**Y** and the manganese carbonyl salts in solution. The ion triplets of MV (*i.e.*, MVX_2 where $X^- = Cl^-$, Br^-, I^-, PF_6^-, OTf^-) are insoluble in this solvent and eliminate the likelihood of MV^{2+} ions being leached out of the zeolite by ion exchange with the added manganese salts. (b) By a similar reasoning, we deliberately avoided the use of acetonitrile, since this polar solvent is capable of leaching cations from the doped zeolite.

(26) The NIR band is also present in crystalline methylviologen cation radical. See Bockman, T. M.; Kochi, J. K. *J. Org. Chem.* **1990**, *55*, 4130.

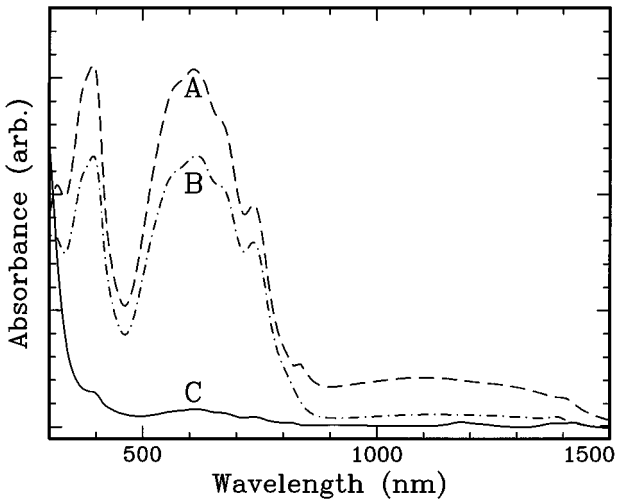

Figure 2. Diffuse reflectance UV−vis−NIR spectra of the blue zeolites-**Y** obtained from the treatment of a THF slurry of MV(1.0)Y with $PPN^+Mn(CO)_5^-$ in the presence of (A) 1.0 equiv, (B) 0.5 equiv, and (C) no added $Na^+BPh_4^-$.

turned blue immediately. However, FT-IR analysis of the supernatant solution revealed the presence of only a negligible amount of $Mn_2(CO)_{10}$, despite the fact that zeolite particles turned blue with significant intensity (especially when suspended in the solvent). Since the amount of $Mn_2(CO)_{10}$ produced was too small to be accurately measured, the reaction was repeated with a large excess of MV(1.0)**Y** (1.0 g containing 0.571 mmol of MV^{2+}) in order to generate more product. Indeed, the careful spectroscopic analysis of the reaction mixture after 0.2 h revealed the presence of only 0.003 mmol of $Mn_2(CO)_{10}$ in the supernatant solution. This redox reaction did not proceed any further, even after a prolonged period of stirring (24 h). Since $Mn_2(CO)_{10}$ contains two carbonylmanganese moieties, the isolated dimer corresponded to the consumption of 0.006 mmol of $Mn(CO)_5^-$, which in return indicated only 1% reduction of the doped MV^{2+} within the zeolite, *i.e.*

$$(MV^{2+})\mathbf{Y} + PPN^+Mn(CO)_5^- \xrightarrow{1\%} (PPN^+MV^{\bullet+})\mathbf{Y} + {}^1/_2Mn_2(CO)_{10} \quad (4)$$

Consistent with this low conversion of MV^{2+} to $MV^{\bullet+}$, the blue color of the zeolite was much weaker, especially in the dried state, compared to the one obtained with $Na^+Mn(CO)_5^-$ (the color appeared rather intense when suspended in the solvent). Indeed, as demonstrated in Figure 2 (curve C), the diffuse reflectance UV−vis analysis showed a much weaker spectrum of $MV^{\bullet+}$ than that of the dark blue colored zeolite obtained with $Na^+Mn(CO)_5^-$. The unreacted $PPN^+Mn(CO)_5^-$ remained intact in the supernatant solution even after 24 h stirring, as demonstrated by the excellent material balance established in Table 2 (entry 3).

It is important to note that the further progress of the redox reaction of MV(1.0)**Y** with $PPN^+Mn(CO)_5^-$ could be deliberately (and precisely) controlled by the addition of an exchangeable sodium ion source to the reaction mixture. For example, when half an equiv of Na^+ BPh_4^- [23] was added to the mixture of $PPN^+Mn(CO)_5^-$ and MV(1.0)**Y**, the zeolite immediately turned deep blue. Spectroscopic analysis of the supernatant solution revealed the presence of $Mn_2(CO)_{10}$ in amounts (0.014 mmol, 0.5 equiv) corresponding to the amount of added sodium salt (entry 4 in Table 2). Further increases in the amount of added Na^+ BPh_4^- [*e.g.*, 0.057 mmol (1 equiv)] led to the quantitative conversion of $Mn(CO)_5^-$ to the dimeric $Mn_2(CO)_{10}$, (0.028 mmol, 1.0 equiv) in the manner previously observed with $Na^+Mn(CO)_5^-$ in eq 3 (see entry 5, Table 2). The dark blue zeolite obtained from the addition of 0.5 equiv of Na^+ BPh_4^- to a mixture of MV(1.0)**Y** and $PPN^+Mn(CO)_5^-$ was visually indistinguishable from that obtained by the addition of 1.0 equiv of Na^+ BPh_4^-. However, quantitative comparison of the diffuse reflectance UV−vis spectra in Figure 2 showed a significant difference in the intensities of the visible absorption band at $\lambda_{max} = 605$ nm.[27]

B. Oxidation of the Phosphite-Substituted Carbonylmanganate Salt $C^+Mn(CO)_4P(OPh)_3^-$ with MV(1.0)Y. The sodium salt of the bulky carbonylmanganate substituted with triphenyl phosphite [*i.e.*, $Na^+Mn(CO)_4P(OPh)_3^-$] was also oxidized by MV(1.0)**Y**, despite the large ligand which prevented its passage through the 7.4-Å window of zeolite-**Y** (see Chart 2). As presented in Table 3, a stoichiometric amount of $Mn_2(CO)_8[P(OPh)_3]_2$ was detected in the supernatant solution immediately after the reaction of MV(1.0)**Y** with this carbonylmanaganate, *i.e.*

$$(MV^{2+})\mathbf{Y} + Na^+Mn(CO)_4P(OPh)_3^- \xrightarrow{100\%} (Na^+MV^{\bullet+})\mathbf{Y} + {}^1/_2Mn_2(CO)_8[P(OPh)_3]_2 \quad (5)$$

By contrast, the large PPN^+ salt of $Mn(CO)_4P(OPh)_3^-$ was inactive, leading to only 1% conversion of the manganese salt into the dimer even after 24 h (cf. eq 3). Moreover, the results in Table 3 show that the addition of Na^+ BPh_4^- sensitively controlled the further oxidation of $Mn(CO)_4P(OPh)_3^-$ by MV(1.0)**Y** in measure with the amount of added sodium ions, in a manner similar to that observed with $PPN^+Mn(CO)_5^-$ (*vide supra*). Thus, the results unambiguously demonstrated that electron transfer occurred readily to the zeolite-encapsulated MV^{2+} acceptor from the large, size-excluded electron donor $Mn(CO)_4P(OPh)_3^-$, as long as Na^+ ion was available.

C. Oxidation of the Medium-Size Tetraethylammonium Salt $TEA^+Mn(CO)_4P(OPh)_3^-$ with MV(1.0)Y. Heretofore, we showed that the redox reactions between MV(1.0)**Y** and $C^+Mn(CO)_4L^-$ [L = CO or $P(OPh)_3$] occurred instantaneously and fell into two categories, *i.e.*, either 100% ($C^+ = Na^+$) or 1% ($C^+ = PPN^+$), simply depending on the size of the counter cation. Since a one-electron reduction must be accompanied by the simultaneous transport of charge-compensating cations, we thought that the *rate* of electron transfer from $Mn(CO)_4P(OPh)_3^-$ in solution to the MV^{2+} ions in the interior of zeolite-**Y** may be governed by the size of the migrating cations. To test this hypothesis, we chose the appropriate medium-size cation $C^+ = TEA^+$ to effect a slower reduction of the zeolite-encapsulated MV^{2+} with $Mn(CO)_4P(OPh)_3^-$. As shown in Table 4, the oxidation of the tetraethylammonium salt $TEA^+Mn(CO)_4P(OPh)_3^-$ indeed proceeded at an intermediate rate compared to that of the sodium salt $Na^+Mn(CO)_4P(OPh)_3^-$. Thus, FT-IR analysis of the reaction mixture showed a gradual growth of the carbonyl bands of the dimer at $\nu_{co} = 2001$ and 1979 (cm^{-1}), at the expense of the carbonyl bands of the monomer ($\nu_{co} = 1962$, 1867, 1842, and 1829 cm^{-1}), as illustrated in Figure 3. Stirring the mixture for extended periods (24 h) ultimately led to about 80% oxidative conversion of $Mn(CO)_4P(OPh)_3^-$ to its dimer. The subsequent addition of a large excess (∼5 equiv) of a sodium salt (Na^+ BPh_4^-) into the incomplete reaction mixture led to an immediate consumption of all the residual manganese anion (see the last entry of Table

(27) (a) Note, however, that the magnitude of the reflectance at $\lambda_{max} = 605$ nm of the half-reduced MV(1.0)**Y** in curve B is higher than one-half that of curve A. (b) Control experiments showed that MV^{2+} was not reduced by $Na^+BPh_4^-$ alone under reaction conditions.

Table 2. Interfacial Electron Transfer between MV(1.0)**Y** and $C^+Mn(CO)_5^-$ Dissolved in THF.[a] Effect of the Cation Size

C^+	time (h)	MV**Y** (g)	$(MV^{2+})^b$	$NaBPh_4$[c]	$Mn_2(CO)_{10}$[d] (conv)[e]	unreacted $Mn(CO)_5^-$ [e]	total Mn mmol (%)
Na^+	0.2	0.1	(0.057)		0.057 (100)	0.006	0.063 (91)
PPN^+	0.2	1.0	(0.571)		0.006 (1)	0.064	0.070 (101)
PPN^+	24	1.0	(0.571)		0.006 (1)	0.063	0.069 (100)
PPN^+	0.2	0.1	(0.057)	0.029	0.029 (51)	0.033	0.062 (89)
PPN^+	0.2	0.1	(0.057)	0.057	0.056 (98)	0.010	0.066 (96)

[a] MV(1.0)**Y** was suspended in 8 mL of THF and 0.069 mmol of $C^+Mn(CO)_5^-$ was added to the slurry. [b] In mmol. [c] Additive, in mmol. [d] In mmol (2×). [e] In %, based on the amount of MV^{2+} in zeolite.

Table 3. Interfacial Electron Transfer between MV(1.0)**Y** and the Phosphite-Substituted Carbonylmanganate Salts $C^+Mn(CO)_4P(OPh)_3^-$.[a] Effect of the Cation Size

C^+	time (h)	MV**Y** (g)	$(MV^{2+})^b$	$NaBPh_4$[c]	$Mn_2(CO)_8P_2$[d] (conv)[e]	unreacted $Mn(CO)_4P^-$ [b,f]	total Mn mmol (%)
Na^+	0.2	0.1	(0.057)		0.057 (100)	0.000	0.057 (100)
PPN^+	0.2	1.0	(0.571)		0.005 (1)	0.052	0.057 (100)
PPN^+	24	1.0	(0.571)		0.005 (1)	0.051	0.056 (98)
PPN^+	0.2	0.1	(0.057)	0.029	0.029 (51)	0.028	0.057 (100)
PPN^+	0.2	0.1	(0.057)	0.059	0.057 (100)	0.000	0.057 100)

[a] MV(1.0)**Y** was suspended in 8 mL of THF and 0.057 mmol of $C^+Mn(CO)_4P(OPh)_3^-$ was added to the slurry. [b] In mmol. [c] Additive, in mmol. [d] In mmol (2×), P represents $P(OPh)_3$. [e] In %, based on the amount of MV^{2+} in zeolite. [f] P = $P(OPh)_3$.

Table 4. Rate Profiles for the Reduction of MV(1.0)**Y** by the Medium-Sized Donor $Et_4N^+Mn(CO)_4P(OPh)_3^-$ [a]

time (h)	$NaBPh_4$[b]	$Mn_2(CO)_8P_2$[c]	(conv)[d]	unreacted Mn[e]	total Mn[e]	mass bal[f]
0.2		0.010	18	0.047	0.057	98
0.5		0.016	28	0.043	0.059	102
1		0.029	51	0.027	0.056	97
3		0.036	63	0.020	0.056	97
5		0.038	67	0.019	0.057	98
7		0.041	72	0.016	0.057	98
24		0.045	79	0.012	0.057	98
0.2[g]	0.292	0.057	100	0.000	0.057	98

[a] 100 mg of MV(1.0)**Y** (MV^{2+} = 0.057 mmol) was suspended in 8 mL of THF, and 35.1 mg (0.058 mmol) of $Et_4N^+Mn(CO)_4P(OPh)_3^-$ was added to the slurry. [b] Additive, in mmol. [c] In mmol (2×), P represents $P(OPh)_3$. [d] Based on the amount of MV^{2+} in zeolite. [e] In mmol; Mn represents $Mn(CO)_4P(OPh)_3^-$. [f] Material balance of the $Mn(CO)_4P(OPh)_3^-$ moiety in %. [g] 0.2 h after the addition of 5 equiv of $Na^+BPh_4^-$ to the reaction mixture.

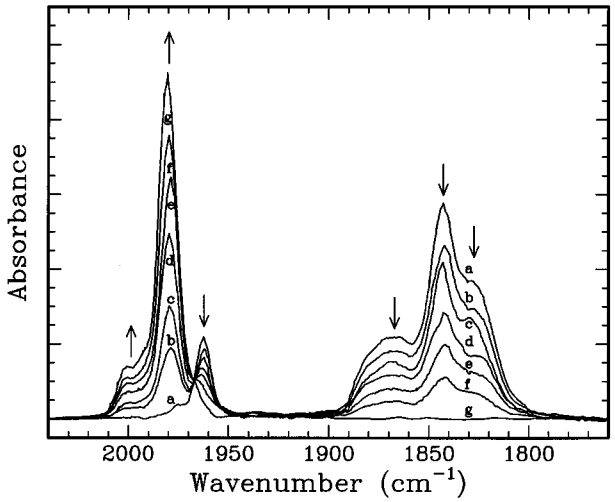

Figure 3. Progressive conversion of $TEA^+Mn(CO)_4P(OPh)_3^-$ into $Mn_2(CO)_8[P(OPh)_3]_2$ followed by FT-IR spectroscopy during the redox reaction with MV(1.0)**Y** in THF with time: t = 0 (a), 0.2 (b), 0.5 (c), 1 (d), 7 (e), 24 h (f). Spectrum (g) was measured at 0.2 h after the addition of $Na^+BPh_4^-$ into the solution of (f).

4). The close examination of the reaction profile further revealed that the redox reaction proceeded in two distinct phases: an initial relatively fast transformation followed by a slower oxidation. For example, roughly 50% of the anion was converted into the dimeric $Mn_2(CO)_4[P(OPh)_3]_2$ during the first hour, but only a small additional conversion (30%) was achieved in the following 23 h period. Figure 4A illustrates the distinctively differentiated reaction (rate) profiles obtained when cations with the progressively increasing size were used, namely, $C^+ = Na^+ \gg TEA^+ \gg PPN^+$. Thus, this figure clearly demonstrated that the size of the counter cation sensitively governed the overall redox rate between the $Mn(CO)_4P(OPh)_3^-$ in solution and the MV^{2+} encapsulated in zeolite-**Y**.

Table 5. Progressive Course of the Interfacial Electron Transfer between MV(2.0)**Y** and $C^+Mn(CO)_4P(OPh)_3^-$.[a] Effect of the Cation Size and the MV^{2+} Occupancy

C^+	time (h)	$Mn_2(CO)_8P_2$[b]	(conv)[c]	unreacted Mn[d]	total Mn[d]	mass bal[e]
Na^+	0.2	0.112	(100)	0.000	0.112	100
Et_4N^+	0.2	0.004	(4)	0.105	0.109	97
Et_4N^+	1	0.012	(11)	0.099	0.111	99
Et_4N^+	3	0.014	(13)	0.095	0.109	97
Et_4N^+	5	0.014	(13)	0.095	0.109	97
Et_4N^+	7	0.014	(13)	0.095	0.109	97
Et_4N^+	24	0.016	(14)	0.094	0.110	98
PPN^+	0.2	0.001	(1)	0.110	0.111	99
PPN^+	24	0.001	(1)	0.111	0.112	100

[a] 100 mg of MV(2.0)**Y** (MV^{2+} = 0.112 mmol) was suspended in 8 mL THF and 68.1 mg (0.112 mmol) of $Et_4N^+Mn(CO)_4P(OPh)_3^-$ was added to the slurry. [b] In mmol (2×), P represents $P(OPh)_3$. [c] In %, based on the amount of MV^{2+} in zeolite. [d] In mmol, Mn represents $Mn(CO)_4P(OPh)_3^-$. [e] Material balance of $Mn(CO)_4P(OPh)_3$ moiety, in %.

D. Oxidation of $C^+Mn(CO)_4P(OPh)_3^-$ with the Highly Doped MV(2.0)Y. The rate of ion migration from the exterior surface into the internal pores of zeolites was also expected to be affected by the number (occupancy) and the size of the preexisting host molecules. Accordingly, we prepared a zeolite-**Y** sample which contained an average of two MV^{2+} cations per supercage [designated as MV(2.0)**Y**] in order to test the effect of the occupancy of the MV^{2+} in the supercage on the degree and the rate of oxidation of $Mn(CO)_4P(OPh)_3^-$. When TEA^+ was employed as the counter cation, the oxidation of the manganese salt with MV(2.0)**Y** only proceeded to less than 15% conversion even after 24 h stirring (Table 5). By contrast, with Na^+ as the counter cation, the production of a stoichiometric (quantitative) amount of manganese dimer was observed within less than 10 min. [Despite the high probability of two $MV^{\bullet+}$ existing within each supercage, the diffuse reflectance spectrum of the blue zeolite was quite similar to the spectrum shown in Figure 2A.[26]] As expected, the oxidative conversion of $PPN^+Mn(CO)_4P(OPh)_3^-$ by MV(2.0)**Y** was limited to 1%.

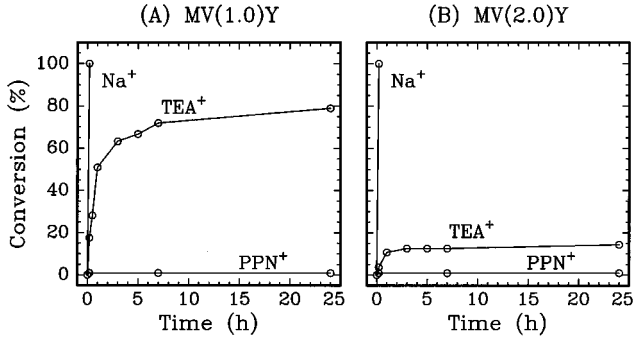

Figure 4. Rate profiles for the oxidative conversion of $Mn(CO)_4P(OPh)_3^-$ to $Mn_2(CO)_8[P(OPh)_3]_2$, showing the effect of the counter cation C^+ (as indicated) and the zeolite occupancy with (A) MV(1.0)**Y** and (B) MV(2.0)**Y** in THF.

Table 6. Kinetics of Interfacial Electron Transfer between MV**Y** and $Na^+Mn(CO)_4P(OPh)_3^-$.[a] Effect of the MV^{2+} Loading

MV( )**Y**	MV^{2+} [b]	Mn^c	time (h)	Mn_2[d]	conv (%)[e]	unreacted Mn	total Mn[f]	mass bal[g]
MV(0.1)**Y**	0.006	0.057	0.2	0.0056	100	0.050	0.056	98
MV(0.2)**Y**	0.012	0.057	0.2	0.010	83	0.045	0.055	96
MV(0.5)**Y**	0.028	0.057	0.2	0.024	86	0.027	0.051	89
MV(1.0)**Y**	0.057	0.057	0.03	0.030	53	0.024	0.054	95
MV(1.0)**Y**	0.057	0.057	0.1	0.046	81	0.007	0.053	93
MV(1.0)**Y**	0.057	0.057	0.2	0.051	89	0.004	0.055	96
MV(1.0)**Y**	0.057	0.057	1.0	0.057	100	0.000	0.057	100
MV(2.0)**Y**	0.112	0.112	0.03	0.084	75	0.027	0.111	99
MV(2.0)**Y**	0.112	0.112	0.1	0.096	86	0.018	0.114	102
MV(2.0)**Y**	0.112	0.112	0.2	0.106	95	0.005	0.111	99
MV(2.0)**Y**	0.112	0.112	1.0	0.112	100	0.000	0.112	100

[a] 100 mg of MV**Y** was suspended in 8 mL of THF. [b] MV^{2+} loading in mmol. [c] Added $Mn(CO)_4P(OPh)_3^-$ in mmol. [d] $Mn_2(CO)_8[P(OPh)_3]_2$ formed in mmol (2×). [e] Conversion (%) based on the amount of MV^{2+} in zeolite. [f] Of $Mn(CO)_4P(OPh)_3^-$ added in mmol. [g] Material balance of $Mn(CO)_4P(OPh)_3^-$ in %.

The three different rate profiles obtained with MV(2.0)**Y** and the carbonylmanganate salts of Na^+, TEA^+, and PPN^+ are compared in Figure 4B, and those observed with MV(1.0)**Y** are shown in Figure 4A. The results show that steric congestion within the zeolite-**Y** supercage further affected the degree and the rate of the redox reaction, the differentiation of which was especially apparent with the medium-sized $TEA^+Mn(CO)_4P(OPh)_3^-$ in Figure 4, A and B.

In order to evaluate the factors controlling the rate of charge propagation with $C^+ = Na^+$, kinetic measurements were also made on a series of MV^{2+} doped zeolite-**Y** with different loading levels of one MV^{2+} per 2, 5, and 10 supercages.[28a] The comparative results in Table 6 show very little difference in the conversion with variations in the loading of MV^{2+} (compare entries 1, 2, 3, 6, and 9). Furthermore, the rate of MV^{2+} reduction in MV(1.0)**Y** was too fast for us to experimentally differentiate it from that in MV(2.0)**Y**, as shown by a direct comparison of the results in Table 6, entries 4−7 with those in entries 8−11.[28b]

Discussion

Pentacarbonymanganate $Mn(CO)_5^-$ is known to be a strong one-electron donor.[28] For example, $Mn(CO)_5^-$ forms highly colored intermolecular 1:1 charge-transfer ion pairs ($\lambda_{CT} > 560$ nm) even with a series of relatively weak pyridinium acceptors such as 4-phenyl-*N*-methylpyridinium ($E_{red} = -1.27$ V vs SCE), *N*-methyl-2-quinolinium ($E_{red} = -1.08$), and 4-carbomethoxy-*N*-pyridinium ($E_{red} = -0.79$ V) in acetonitrile solution.[29a] In this regard, the electron transfer (Table 1, eq 1) between the carbonylmanganate and MV^{2+} ion is expected to be enhanced owing to the much stronger acceptor strength of the bipyridinium ion ($E_{red} = -0.45$ vs SCE in CH_3CN).[15] Previous studies with pyridinium acceptors showed that the redox reaction in eq 1 derives from the stepwise mechanism,[29b] *i.e.*

$$MV^{2+} + Mn(CO)_5^- \xrightarrow{k_{ET}} MV^{\bullet+} + Mn(CO)_5^{\bullet} \quad (6)$$

$$2Mn(CO)_5^{\bullet} \xrightarrow{\text{fast}} Mn_2(CO)_{10} \quad (7)$$

where k_{ET} denotes the rate-limiting electron transfer step. The instantaneous redox reaction in eq 1 indicates that electron transfer between MV^{2+} and $Mn(CO)_5^-$ is rapid, since the subsequent dimerization step of the manganese carbonyl radical is known to be diffusion controlled.[30] [The quantitative formation of dimeric $Mn_2(CO)_{10}$ is consistent with the substitution inertness of the manganese carbonyl radical under the reaction conditions.] Coupled with the high stability of $MV^{\bullet+}$, let us now consider the merits of using carbonylmanaganate as the electron donor paired with C^+ (as described in the Introduction) for the study of electron transfer across the zeolite surface.

Our previous work established that only the donors that can fit through the zeolite pores can effectively interact with the preloaded acceptors to form electron donor−acceptor complexes within the zeolite supercage.[2,18,19,31] Likewise, for this electron transfer study, only those carbonylmanganate reducing agents that can be admitted into the zeolite supercage are expected to react with the zeolite-encapsulated methylviologen. Thus, the immediate as well as quantitative redox reaction that occurs between the size-excluded $Na^+Mn(CO)_4P(OPh)_3^-$ salt and the zeolite-intercalated MV^{2+} ions (Table 3) appears to be highly anomalous at first glance, since such a large anion as $Mn(CO)_4P(OPh)_3^-$ is subject to zeolite shape selectivity.[32] Furthermore, the occurrence of the fast redox reaction between $Na^+Mn(CO)_4P(OPh)_3^-$ and the highly congested MV(2.0)**Y** with two large MV^{2+} ions (again instantaneously and quantitatively), strongly suggests that some *non-shape selective* pathway must

Table 7. Diagnostic IR bands of the Metal Carbonyls[a]

compound	IR stretching band (cm^{-1})
$Na^+Mn(CO)_5^-$	2013(vw), 1897, 1872(sh), 1863, 1832(w)
$TMA^+Mn(CO)_5^-$	2013(vw), 1898, 1866, ∼1851(sh)
$TEA^+Mn(CO)_5^-$	2012(vw), 1898, 1865, ∼1851(sh)
$TBA^+Mn(CO)_5^-$	2012(vvw), 1869, 1863
$PPN^+Mn(CO)_5^-$	1894, 1862
$PPh_4^+Mn(CO)_5^-$	1894, 1862
$Na^+Mn(CO)_4P(OPh)_3^-$	1964, 1877, 1850, 1804
$TEA^+Mn(CO)_4P(OPh)_3^-$	1963, 1867(sh), 1842, 1829
$PPN^+Mn(CO)_4P(OPh)_3^-$	1962, 1871, 1840
$Mn_2(CO)_8[P(OPh)_3]_2$	2001(vw), 1979

[a] In THF solution.

(28) (a) We thank a referee for suggesting these experiments. (b) At short reaction times, the measured conversions in Table 6 were subject to considerable uncertainty (±10%) owing to the experimental difficulties in efficient filtration when $t < 10$ min.

(29) (a) Bockman, T. M.; Kochi, J. K. *J. Am. Chem. Soc.* **1989**, *111*, 4669. (b) See: Lehman, R. E.; Bockman, T. M.; Kochi, J. K. *J. Am. Chem. Soc.* **1990**, *112*, 458. Kochi, J. K; Bockman, T. M. *Adv. Organometal. Chem.* **1991**, *33*, 51.

(30) (a) Waltz, W. L.; Hackelberg, O.; Dofman, L. M.; Wojcicki, A. *J. Am. Chem. Soc.* **1978**, *100*, 7259. (b) Walker, H. W.; Herrick, R. S.; Olsen, R. J.; Brown, T. L. *Inorg. Chem.* **1984**, *23*, 3748.

(31) (a) Yoon, K. B.; Kochi, J. K. *J. Am. Chem. Soc.* **1989**, *111*, 1128. (b) Yoon, K. B.; Huh, T. J.; Corbin, D. R.; Kochi, J. K. *J. Phys. Chem.* **1993**, *97*, 6492. (c) Yoon, K. B.; Huh, T. J.; Kochi, J. K. *J. Phys. Chem.* **1995**, *99*, 7042.

(32) Csicsery, S. M. in *Zeolite Chemistry and Catalysis*; Rabo, J. A. Ed.; ACS Monograph 171; American Chemical Society: Washington, DC, 1976; pp 680 ff.

be operating. Among the various (possible) explanations, we favor a mechanism in which *electrons* are initially transferred from the external, size-excluded carbonylmanaganate donor to a zeolite-encapsulated methylviologen acceptor,[33] and then they migrate through the zeolite framework. In other words, we believe electron conduction is responsible for the non-shape selective behavior. Alternatively, one might suspect that the anomalous behavior could arise from the prior substitution of the bulky $P(OPh)_3$ ligand by the smaller THF solvent molecule to generate $Mn(CO)_4THF^-$ which could then be admitted into the supercage of zeolite-**Y**. However, the instantaneous and quantitative formation of the dimeric $Mn_2(CO)_8[P(OPh)_3]_2$ as the sole product eliminates this possibility. Furthermore, the results in Table 3 show that the unreacted $PPN^+Mn(CO)_4P(OPh)_3^-$ remains structurally intact even when it is exposed to THF for prolonged periods (entry 3, as well as the last entry in Table 5), which demonstrates that this manganese anion is stable and substitution inert under the reaction conditions.

Although the unsubstituted manganese carbonyl anion $Mn(CO)_5^-$ is able to freely enter the zeolite-**Y** supercage to effect electron transfer with MV^{2+} (see Chart 2), the redox reaction between $Na^+Mn(CO)_5^-$ with MV(1.0)**Y** rapidly produces the dimeric $Mn_2(CO)_{10}$ in quantitative amounts *only in the supernatant solution* (entry 1, Table 2). This important observation also indicates that electron conduction through the zeolite occurs after the carbonylmanganate donor is externally oxidized by MV^{2+} at the surface. Such a mechanistic view is especially attractive for the redox reaction between $Na^+Mn(CO)_5^-$ and the highly loaded MV(2.0)**Y**, whose supercages are unlikely to accommodate an additional (carbonylmanganate) guest since they are already congested with two methylviologen moieties.

In order to ensure charge balance, however, electron conduction requires the transport of positive charge from the external surface into the internal supercages. Unlike electrons, however, the transport of cations from the zeolite exterior into the internal framework is subject to zeolite shape selectivity,[32] owing to their much larger, definitive shapes. Accordingly, we attribute the limited conversion (<1%) consistently observed with the PPN^+ salts of carbonylmanganates (see Tables 2, 3, and 5) to the inability of this cation to be transported into the supercage, owing to its large size. Such a size restriction of PPN^+ (relative to Na^+) during electron transfer to MV^{2+} is pictorially represented in Chart 4. In fact, the limited conversion of $PPN^+Mn(CO)_4L^-$ to an extent of 1% is quite revealing, if we recall that the number of outermost (peripheral) supercages in zeolite-**Y** corresponds to about 1% of the total number of supercages.[36] As such, we attribute the very low (1%) conversion of methylviologen with $PPN^+Mn(CO)_4L^-$ to the reduction of only those MV^{2+} ions that exist within the peripheral supercages of the zeolite microcrystals. Note that the large size-excluded PPN^+ cations are likely to remain in the vicinity of the external surface in order to fulfill the charge balance. If so, this represents a unique example in which electron transfer occurs solely in the zeolite supercages that lie on the crystal surface. This formulation also predicts that charge separation between the size-excluded cation and the zeolite-intercalated reduced species may be achieved at the monolayer level.

Chart 4. Size exclusion of the large cation PPN^+ from the supercage of zeolite-**Y** during electron-transfer reduction of methylviologen.

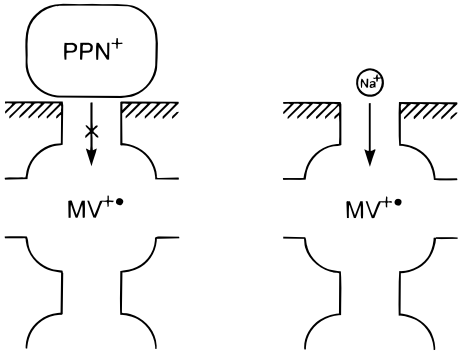

Consistent with this picture, we propose that the migration of the cation (C^+) from the exterior into the internal supercages is also responsible for the observed slow progress of the reaction of the medium-sized TEA^+ salt of $Mn(CO)_4P(OPh)_3^-$ with MV(1.0)**Y**. The effect is even more apparent with the highly loaded MV(2.0)**Y**, as illustrated in Figure 4. This conclusion favors intrazeolite transport of the relatively small Na^+ ions to occur quite rapidly—even through the highly congested MV(2.0)**Y**. Furthermore, the incomplete conversions observed with $TEA^+Mn(CO)_4P(OPh)_3^-$ [*i.e.*, 79% over MV(1.0)**Y** and 14% over MV(2.0)**Y**, even after stirring for 24 h] suggest that the remaining free space of the acceptor-doped supercage also controls the progress of the electron transport. Likewise, the rather slow reaction observed between the insoluble crystalline salt $MV(OTf)_2$ and $PPN^+Mn(CO)_4L^-$ [Table 1, L = CO or $P(OPh)_3$] in THF suspension can be attributed to the absence of an appropriate channel (*i.e.*, void space) within the crystalline solid for the simultaneous transport of the counter cation during the redox reaction.

According to our formulation, both electrons and cations must be propagated from the exterior surface into the zeolite interior in order to effect complete electron transfer between the dissolved manganese donors and all the intercalated MV^{2+} acceptors.[37] Although cations must move from one supercage to another during the redox reactions, our experimental results do not provide a direct mechanism as to how the electrons actually migrate from the exterior surface into the interior supercages. An attractive possibility is for electron transfer to occur from a methylviologen cation radical ($MV^{\bullet+}$) in one supercage to a dicationic methylviologen (MV^{2+}) in one of the neighboring supercages by a direct contact through the interconnecting windows,[38] *i.e.*

(33) The driving force for electron transfer is $\Delta G \sim 5$ kcal mol^{-1} based on the oxidation potential of $Mn(CO)_5^-$ (−0.25 V vs SCE)[34] and the reduction potential of MV^{2+} (−0.45 V)[35] in acetonitrile.

(34) Tilset, M.; Parker, V. D. *J. Am. Chem. Soc.* **1989**, *111*, 6711.

(35) The oxidation potential of MV^{2+} has been shown to vary depending on the polarity of medium. Thus the E°_{red} values of MV^{2+} are −0.45 in CH_3CN, −0.43 in DMF, and −0.68 in water (vs SCE). However, from an estimation of the zeolite polarity to be similar to the mixture of water and acetonitrile (see: Yoon, K. B.; Kochi, J. K. *J. Am. Chem. Soc.* **1988**, *110*, 6586), the oxidation potential of MV^{2+} can be approximated to be −0.5 V.

(36) The total number of supercages (N_t) can be estimated by assuming that each supercage occupies a 13 Å cube. The ratio of the number of outermost supercages (N_o) to N_t depends on the zeolite-**Y** particle size, and N_o/N_t is estimated to be 0.01_1 for the average crystal size (0.7 micron) of the zeolite-**Y** samples used in this study.

(37) The related electron transport from the electrode to the zeolite-encapsulated substrates accompanied by cation transport into the zeolite interior has been proposed from studies of zeolite-modified electrodes.[8−10] [In this regard, the carbonylmanganate donors $Mn(CO)_4L^-$ (L = CO and $P(OPh)_3$)] can be likened to a cathode.] However, the electrochemical methods suffer from various problems[8] associated with the fabrication of zeolite modified electrodes and, in particular, the use of highly concentrated electrolytic solutions which commonly leach out the electroactively charged species from the zeolite.

(38) (a) The electron transfer through the window between the molecules encapsulated in the neighboring supercages has also been proposed in other systems. See refs 4b and 6. (b) The results in Table 6 show that Na^+ migration through zeolite-**Y** was too fast for us to distinguish the kinetic order for the reduction of MV^{2+}.

$$(C^+, MV^{\bullet+})_{sc_1} + (MV^{2+})_{sc_2} \leftrightarrows (MV^{2+})_{sc_1} + (C^+, MV^{\bullet+})_{sc_2}, \text{ etc.} \quad (8)$$

where the subscript sc_1 represents the outermost supercage, and sc_2 the neighboring supercage, etc. The subsequent propagation of the electron through the neighboring zeolite supercages based on this scheme is schematically depicted in Chart 5. A less attractive possibility involves the sequential migration of $MV^{\bullet+}$ out of sc_1 into the neighboring supercage (sc_2) that is accompanied by the reverse migration of MV^{2+} into sc_1, etc. However, the simultaneous movement of the relatively large methylviologen mono- and dications through the narrow (7.4 Å aperture) windows of zeolite-**Y** depicted in Chart 1 is expected to be prohibitively slow.

Summary and Conclusion

Interfacial electron transfer to a zeolite-intercalated cationic acceptor proceeds equally well, even from size-excluded donors, but it is adversely affected by the large sizes/shapes of charge-balancing cations. Thus, the one-electron reduction of methylviologen encapsulated in zeolite-**Y** particles (containing either 1 or 2 MV^{2+} per supercage) by the sodium carbonylmanganates $Na^+Mn(CO)_4L^-$ with L = CO or $P(OPh)_3$ occurs rapidly and quantitatively, *i.e.*

$$(MV^{2+})\mathbf{Y} + Mn(CO)_4L^- \xrightarrow[THF]{} (MV^{\bullet+})\mathbf{Y} + Mn(CO)_4L^{\bullet}$$

despite the fact that the triphenyl phosphite-substituted donor is too large to penetrate the zeolite aperture as depicted in Chart 2. In both cases, the reduced methylviologen cation radical is observed as very dark blue zeolite particles, and the oxidized (17-electron) carbonylmanaganese radical is quantitatively isolated from the supernatant solution as the dimeric $Mn_2(CO)_{10}$ or $Mn_2(CO)_8[P(OPh)_3]_2$. In strong contrast, the same carbonylmanganates as the size-excluded PPN^+ salts are ineffective donors, and they can reduce only a small fraction of the methylviologen, *i.e.*, (1%) corresponding to the MV^{2+} located in the outermost supercages of the zeolite particles.

The surprising efficiency of the size-excluded donor $Mn(CO)_4P(OPh)_3^-$, coupled with the absence of reduced $Mn(CO)_4L^{\bullet}$ species within the zeolite particles, indicates that reduction proceeds via an interfacial electron transfer from $Mn(CO)_4L^-$ in solution to only that MV^{2+} in the peripheral supercages. As such, the complete reduction of every intercalated (MV^{2+}) acceptor requires a mechanism for electron conduction into the interior of the zeolite particle. Indeed, the shape-selective behavior of the charge-compensating cations C^+ (compare eq 3 with eq 4) accounts for their simultaneous transport, as the reduced ($MV^{\bullet+}$) center migrates throughout the zeolite framework in Chart 5. Such a cation-modulated electron conduction must be rapid to account for the instantaneous and quantitative reduction of every methylviologen acceptor in MV(1.0)**Y** according to eqs 3 and 5, as well as the doubly occupied MV(2.0)**Y** in entry 1, Table 5 [provided, of course, that C^+ is sufficiently small (like Na^+) to readily penetrate the MV^{2+}-doped zeolite-**Y**]. In a related vein, Shaw and co-workers[39] previously reported that electrolyte cations also show shape-selective behavior in electron conduction through zeolite-modified electrodes in cyclic voltammetric studies. Although their mechanistic delineation was complicated by the competitive leaching of the charged species from the zeolite into the highly concentrated electrolytic solutions,[40] our studies establish electron transfer/cation transport as described in Chart 5 to be the highly efficient process for electron conduction. Moreover, a similar consideration may be applicable in the use of zeolites to achieve long-lived charge separation during photoinduced electron transfer,[41] and in the reduction of transition-metal complexes exchanged into zeolites for heterogeneous catalysis.[42]

Chart 5. Electron-conduction mechanism for the propagation of $MV^{\bullet+}$ through zeolite supercages, showing the accompanying transport of the counter cation C^+.

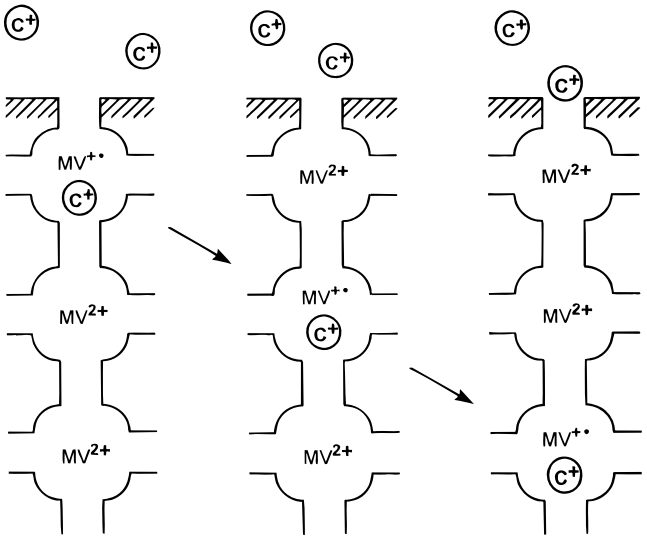

Experimental Section

Materials. Zeolite-**Y** (LZY-52, Lot No. 968087061020-S) from Union Carbide was washed with aqueous 1 M NaCl solution and subsequently treated with distilled deionized water until the silver ion test for chloride was negative. The zeolite was then dried in air to allow equilibration with atmospheric moisture. The average size of the zeolite-**Y** particle was 0.7 μ as determined from the scanning electron micrograph (SEM). Methylviologen dichloride ($MVCl_2$) from Hannong Chemical was recrystallized repeatedly from methanol until colorless. The triflate salt of MV^{2+} was prepared from 4,4′-bipyridyl with methyl trifluoromethanesulfonate in dichloromethane. $MV(OTf)_2$: ^1H NMR (CD_3CN), δ 8.84 (d, J_{HH} = 4 Hz, 4 H), 8.36 (d, J_{HH} = 4.8 Hz, 4 H), 4.39 (s, 6 H). All air-sensitive metal carbonyl compounds were handled and stored in a glovebox charged with high purity argon or in Schlenk tubes under an argon atmosphere. The characteristic FT-IR carbonyl stretching bands of the carbonylmanganate compounds are listed in Table 7. $Mn_2(CO)_{10}$ from Strem was recrystallized from toluene by cooling the saturated solution to −35 °C, and then stored in a glovebox. The sodium salt of $Mn(CO)_5^-$ was prepared from $Mn_2(CO)_{10}$ by treating with sodium amalgam (Na/Hg)

(39) Shaw, B. R.; Creasy, K. E.; Lanczycki, C. J.; Sargeant, J. A.; Tirhado, M. *J. Electrochem. Soc*. **1988**, *135*, 869.

(40) For a review, see: Bard, A. J.; Mallouk, T. *Techniques of Chemistry, Molecular Design of Electrode Surfaces*; Murray, R. W., Ed.; Wiley: New York, 1992; Vol. XXII, Chapter 6.

(41) (a) Ramamurthy, V., Ed.; *Photochemistry in Organized and Constrained Media*; VCH: New York, 1991. (b) Holt, S. L., Ed. *Inorganic Reactions in Organized Media*; ACS Symposium Series 177; American Chemical Society: Washington, DC, 1981.

(42) (a) Minachev, K. M.; Isakov, Y. I. In *Zeolite Chemistry and Catalysis*: Rabo, J. A,, Ed.; ACS Monograph 171; American Chemical Society: Washington, DC, 1976; p 552. (b) Chen, N. Y.; Garwood, W. E.; Dwyer, F. G. *Shape Selective Catalysis in Industrial Applications;* Marcel Dekker: New York, 1989. (c) Rabo, J. A.; Angell, C. L.; Kasai, P. H.; Schomaker, V. *Discuss. Faraday Soc*. **1966**, *41*, 328. (d) Park, Y. S.; Lee. Y. S.; Yoon, K. B. *J. Am. Chem. Soc*. **1993**, *115*, 12220. (e) Kasai, P. H.; Bishop, R. J., Jr. *J. Phys. Chem*. **1973**, *77*, 2308. (f) Westphal, U.; Geismar, G. *Z. Anorg. Allg. Chem*. **1984**, *508*, 165. (g) Anderson, P. A.; Edwards, P. P. *J. Am. Chem. Soc*. **1992**, *114*, 10608. (h) Haug, K.; Srdanov, V.; Stucky, G. Metiu, H. *J. Chem. Phys*. **1992**, *96*, 3495. (i) Sun, T.; Seff, K.; Heo, N. H.; Petranovskii, V. P. *Science*, **1993**, *259*, 495. (j) See also ref 1a.

in THF. The complete conversion of the dimer to $Mn(CO)_5^-$ was spectrally monitored by FT-IR analysis. The yellow solution was separated from the mercury residue with the help of a disposable pipet and filtered through a glass frit. The product was isolated by adding excess *n*-hexane into the THF solution. The yellow powder was recrystallized at −35 °C by the gradual addition of *n*-hexane into the THF solution (until cloudy). The sodium salt was metathesized with 1 equiv of each chloride salt of tetramethylammonium (TMA^+, Matheson, Coleman and Bell), tetraethylammonium (TEA^+, Aldrich), tetra-*n*-butylammonium (TBA^+, Aldrich), bis(triphenylphosphine)-iminium (PPN^+, Aldrich), and tetraphenylphosphonium (PPh_4^+, Aldrich), respectively, in THF by stirring for 2−3 h. NaCl was removed by filtration and *n*-hexane was added to each clear yellow solution to isolate yellow powders. The salts were similarly purified by recrystallization. $Mn_2(CO)_8[P(OPh)_3]_2$ was prepared by irradiating a *n*-hexane solution (200 mL) of $Mn_2(CO)_{10}$ (7 g, 0.018 mol) and triphenyl phosphite $P(OPh)_3$, (16.7 g 0.054 mol, Aldrich) in a Rayonet photochemical reactor (using 350-nm tubes) under argon.[43] The reaction mixture was contained in a Pyrex Schlenk flask. Orange crystals slowly formed over the period of 2 days, and the filtered orange crystals were washed with *n*-hexane. This procedure not only resulted in a very pure product, but it also afforded higher yields than the reported thermal methods.[44] The sodium salt of $Mn(CO)_4P(OPh)_3^-$ was prepared by treating $Mn_2(CO)_8[P(OPh)_3]_2$ with sodium amalgam (Na/Hg) in THF. The salt was isolated by adding excess *n*-hexane into the filtered solution, and purified by adapting the method applied for $Na^+Mn(CO)_5^-$. The TEA^+ and PPN^+ salts of $Mn(CO)_4P(OPh)_3^-$ were prepared from $Na^+Mn(CO)_4P(OPh)_3^-$ by metathesizing sodium ion with the corresponding cation using TEA^+Cl^- and PPN^+Cl^-, respectively. The TEA^+ and PPN^+ salts of $Mn(CO)_4P(OPh)_3^-$ were similarly purified by recrystallizing the corresponding salt in a mixed solvent of THF and *n*-hexane at −35 °C. TMA^+Cl^-, TEA^+Cl^-, and TBA^+Cl^- were dried at 100 °C for 15 h in vaccuo. Na^+ BPh_4^- from Aldrich was used as received. All the purified solvents were stored in Schlenk flasks under argon and kept in the glovebox. Tetrahydrofuran (THF) and diethyl ether were purified by distillation over sodiobenzophenone. Acetonitrile was stirred over potassium premanganate for 15 h at room temperature and then separated by filtration. The permanganate treated acetonitrile was distilled, and the distillate was then refluxed and redistilled over phosphorus pentoxide under an argon atmosphere. *n*-Hexane was stirred repeatedly with sulfuric acid until the acid layer remained colorless. The separated solvent was then washed with water and subsequently with dilute aqueous sodium bicarbonate solution. The washed *n*-hexane was dried with anhydrous calcium chloride and distilled from sodium under an argon atmosphere.

Preparation of MV^{2+}-Doped Zeolites-Y. The MV^{2+}-doped zeolites-**Y** were prepared by the aqueous ion exchange of sodium zeolite-**Y** with MV^{2+} ions. The amounts of MV^{2+} ions intercalated in zeolite-**Y** were controlled to be 0.1, 0.2, 0.5, 1.0, and 2.0 per supercage. Typically, MV(1.0)**Y** (zeolite-**Y** exchanged with 1 MV^{2+} per supercage on an average basis) was obtained by adding 1.13 g (4.65 mmol) of $MVC1_2$ into a slurry containing 10 g of Na**Y** (4.64 mmol of supercage) and 0.9 L of distilled deionized water in a 1-L flask. The slurry was then shaken for 15 h at ambient temperature. The resultant MV^{2+}-doped zeolite-**Y** was filtered through a sintered glass filter and washed with copious amounts of water until the chloride test with $AgNO_3$ was negative. The amounts of unexchanged MV^{2+} ion in the combined wash were quantified by UV−vis spectrophotometry monitored at $\lambda_{max} = 257$ nm ($\epsilon = 20\,417$).[13] Quantitative analysis revealed that essentially all the added MV^{2+} ion was exchanged into the zeolite. MV(2.0)**Y** was prepared by a two-step exchange. The first exchange was carried out by shaking 5 g of Na**Y** (2.32 mmol of supercage) and 0.76 g of $MVC1_2$ (3.12 mmol) in 500 mL of water. Quantitative analysis showed that almost all the MV^{2+} ions were exchanged into Na**Y** (1.34 MV^{2+} per supercage) from the first exchange. The second exchange was carried out by shaking the MV^{2+}-doped zeolite and 0.55 g of $MVC1_2$ (2.26 mmol) in 500 mL of water. The degree of acceptor incorporation reached slightly more than 2.0 MV^{2+} per supercage after the second exchange. The MV^{2+}-doped zeolites were first dried in air at ambient temperatures. The air-dried zeolites were then evacuated at 25 °C for 2 h under vacuum ($<10^{-5}$ torr). The temperature of MV(1.0)**Y** was slowly increased to 150 °C over a period of 2 h, and they were evacuated further at this temperature for an additional 10 h. The maximum dehydration temperature for MV(2.0)**Y** was 100 °C since the acceptor-doped zeolite turned pale blue at higher temperatures. All the dried zeolites were transferred into an argon-filled glovebox and kept in the glass-stoppered containers.

Oxidation of Carbonylmanganates with MV^{2+}-Doped Zeolites-Y. Typically, THF (1 mL) was added to a glass vial (15 mL capacity) containing a weighed amount (0.1 or 1.0 g) of an acceptor-doped zeolite in order to soak the powders. Generation of heat was usually noticed when the relatively polar solvent was added to the zeolites. A required amount of the carbonylmanganate was weighed into a separate vial and 5 mL of THF was added. The metal carbonyl solution was then introduced into the vial containing zeolite with the aid of a pipet. The vial used for the preparation of metal carbonyl was washed twice with an additional 1 mL of the solvent. Each of the washed solvent was also transferred into the reaction vial. A small Teflon-coated magnetic stirring bar was added into the reaction vessel and then the slurry was stirred with the aid of a magnetic stirrer for the desired length of time.

The reaction mixture was filtered by passing it through a cotton-packed glass column. The cotton-packed column was previously washed with solvent and dried. The packed cotton did not affect the carbonylmanganates used in this study. The filtered solution was collected into a 25- or 50-mL volumetric flask. The reaction vial was washed repeatedly with small amounts of fresh solvent and each washed solvent was passed through the (filtered) zeolite cake. Washing the filtered zeolites was continued until the collected solution accumulated to approximately 20 mL for dilute reaction mixtures (25-mL volumetric flask) or about 30 mL for concentrated reaction mixtures (50-mL volumetric flask). After filling the volumetric flask to the marked point with an additional amount of fresh solvent, the collected solution was quantitatively analyzed by FT-IR spectrophotometry. The products were identified by spectral comparisons with the authentic samples. They were quantified (±5%) by comparison with the calibration curves independently constructed from IR absorbencies of the characteristic band vs concentration. For the qualitative visual experiment, a large excess (about 10 molar excess with respect to the amount of acceptor) of manganese carbonyl compounds was added into each zeolite slurry consisting of approximately 0.1 g in 5 mL of solvent.

Instrumentation. FT-IR spectra were obtained with a NaCl liquid cell (0.1 mm) on a Nicolet 10 DX FT spectrometer with 2 cm^{-1} resolution. ^1H NMR spectra were recorded on a JEOL FX 90Q FT spectrometer operating at 89.55 MHz. The diffuse reflectance spectra of the colored zeolites were measured on a Shimadzu UV-3101PC spectrometer equipped with an integrating sphere. The scanning electron micrograph of zeolite-**Y** was obtained on a JEOL JSM-35C microscope.

Acknowledgment. K.B.Y. thanks the R. A. Welch Foundation for financial support during the sabbatical leave in Houston. This research was also carried out under the auspices of the NSF-KOSEF sponsored United States/Korea Cooperative Research Program and the Aimed Basic Research Program of KOSEF. We thank T. M. Bockman for many helpful discussions.

JA962645Y

(43) Osborne, A. G.; Stiddard, M. H. B. *J. Chem. Soc.* **1964**, 643.

(44) (a) Hieber, W.; Freyer, W. *Chem. Ber*. **1959**, *92*, 1765. (b) Lewis, J.; Manning, A. R.; Miller, J. R. *J. Chem. Soc. A* **1966**, 845. (c) Drew, D.; Darensbourg, D. J.; Darensbourg, M. Y. *Inorg. Chem*., **1975**, *14*, 1579.